Available online at www.sciencedirect.com
SCIENCE DIRECT
Journal of the European Ceramic Society 26 (2006) 923–932
www.elsevier.com/locate/jeurceramsoc

Sintering of nanocrystalline Ta_2O_5 and ZrO_2 films compared to that of TiO_2 films

Stéphane Bertaux[a,b], Peter Reynders[b,*], Jean-Marc Heintz[a,1]

[a] *Institute of Condensed Matter Chemistry of Bordeaux, ICMCB-CNRS, University Bordeaux 1, 33608 Pessac, France*
[b] *Merck KGaA, Pigments R&D, Frankfurter Strasse 250, 64293 Darmstadt, Germany*

Received 26 May 2004; received in revised form 15 November 2004; accepted 26 November 2004
Available online 21 January 2005

Abstract

Thin ($d = 60$ nm/140 nm) nanocrystalline Ta_2O_5 and ZrO_2 films were deposited onto SiO_2 flakes, using a liquid route synthesis. Their sintering behaviour was characterized and compared to that of the corresponding powders and the known equivalent TiO_2 film in terms of grain size, grain growth and layer porosity. The effect of the substrate was noticeable on crystallisation process but not on grain growth. The sintering behaviour was actually dictated by the initial size and the packing of the precipitated grains related to the synthesis of the film.

Keywords: Films; Grain growth; Sintering; Ta_2O_5; ZrO_2; TiO_2

1. Introduction

Thin oxide films are today widely used. For example, tantalum oxide is known as a high-quality dielectric material for capacitor technology.[1] It is also used as electroluminescent and filed emission displays,[2] optical[3] and corrosion resistant coatings.[4] For their part, ZrO_2 films have been proposed to be used as thermal barrier coatings for metal components,[5] wear resistant coatings,[6,7] sensor layers,[8–10] dielectric[11] and fuel cell films.[12–15]

The area of optics is obviously another field of current investigations. A good example is the class of nacreous or pearlescent pigments that were originally developed to simulate the appearance of natural pearls. Now, they are incorporated in various industrial products for functional (security printing, optical filter) or decorative purposes (cosmetics, car paints).[16] They are made of thin platelets of high refractive index, which partially reflect and partially transmit light.[17] The lustrous, brilliant or iridescent colour effects are obtained by interference effects on these thin films.[18,19]

The breakthrough for the development of nacreous pigments was done when the deposition of thin metal oxide films was obtained in a controlled way on a substrate, i.e. mica (muscovite). Two main preparation processes have been largely developed. CVD methods are suitable for forming dense oxide films.[20–23] However, this technique is considered as too expensive for industrial pigments. Chemical methods, such as sol–gel or precipitation, are the other possible routes.

The two main oxide films used as nacreous pigments are Fe_2O_3 and TiO_2.[23–26] New improvements have been achieved recently with the use of new synthetic substrates, such as SiO_2 flakes which present an homogeneous thickness, unlike mica flakes which are obtained by a milling/grinding process.[27] Now, TiO_2/mica or TiO_2/SiO_2 pigments are currently prepared via an aqueous precipitation process.[28]

The next step of the preparation of a pearlescent pigment deals with the conversion of the precipitated film into the final oxide, which is usually obtained through a sintering treatment. In fact, such a thermal treatment of a particulate film attached to a rigid substrate corresponds to a constrained sintering problem. Many experimental and theoretical works have been done on that topic.[29–34] In the present case, some interesting developments arise from the nanometric grain size within the film and the nature of the substrate.

* Corresponding author. Tel.: +49 6151 726004; fax: +49 6151 72916004.
E-mail address: peter.reynders@merck.de (P. Reynders).
[1] Member, European Ceramic Society.

0955-2219/$ – see front matter © 2004 Elsevier Ltd. All rights reserved.
doi:10.1016/j.jeurceramsoc.2004.11.019

Yet, several questions are still unsolved, especially about the role of the substrate on grain growth within the thin oxide layer. Part of this problem has been addressed with the grain growth study of Fe_2O_3 special effect pigments with different substrates.[35]

The present study aims to describe the sintering behaviour of pearlescent pigments based on Ta_2O_5 and ZrO_2 films. Although tantalum oxide and zirconia based special effect pigments as well as weather-resistant pearlescent pigment are mentioned in the patent literature,[27,36–40] no large investigation of the film microstructural changes during sintering was reported. Therefore, the first part of this work concerns the characterization of the thermal behaviour (crystallisation, surface area, grain growth) of the as-obtained oxide layers. The second part is related to the comparison of their sintering behaviour to that of nanosized Ta_2O_5 and ZrO_2 powder and known equivalent TiO_2 pigments, in terms of grain size, grain growth and constrained sintering.

2. Experimental procedure

2.1. Powder preparation

The tantalum, zirconium and titanium oxide layers were deposited onto SiO_2 flakes (Merck, diameter 10–50 μm, thickness 450 nm ± 10 nm) via an aqueous liquid deposition process (LPD). It corresponds to the controlled precipitation, at low pH, of the metal chloride within an aqueous suspension containing the substrates. The details are given elsewhere.[41] The thickness of the layers can be controlled by varying the amount of metal chloride solutions used in the LPD. The precipitates were filtered off, washed completely with deionized water and dried at 110 °C for 12 h. Two different film thicknesses (for dried pigments) were considered for the present study: $t = 60$ nm and $t = 140$ nm, respectively called Ta60, Zr60 and Ti60 and respectively Ta140, Zr140 and Ti140 films. Using the same conditions, Ta_2O_5, ZrO_2 and TiO_2 powders were precipitated without any substrate.

All dried pigments were then calcined at different temperatures between 500 and 1150 °C under air for 30 min.

2.2. Powder characterization

X-ray analyses were carried out under air from room temperature to 1200 °C. The pigments were put on a Pt/Rh ribbon. The measurements were carried out in reflection geometry with a θ/θ-diffractometer (Cu Kα, HT-Chamber J. Otto GmbH, Hechingen). The crystallite size was estimated from the full width at half-maximum of diffraction peaks by the Scherrer equation after subtracting the instrumental broadening ($d = 1.04\lambda/[B - b]\cos\theta$, where λ is the X-ray wavelength (0.1541 nm), θ the scattering angle of peaks, B the measured half-maximum width and b the instrumental broadening (0.080°)).

Light microscopy micrographs of the samples were taken using an Eclipse ME 600 (Nikon GmbH) under transmission and reflection conditions.

The morphology of the particles was studied using scanning electron microscopy (SEM) (LEO 1530 Gemini). SEM was also used to measure the layer thickness on micrographs of fractured pigments. The pigments were mixed with a lacquer and dried. The lacquer, containing the pigments, was then broken in such a way that some of the SiO_2 flakes were also broken which allowed the thickness of the coated film to be measured.

The Brunauer–Emmett–Teller (BET) specific surface areas and the pore volumes were measured using a Micromeritics ASAP 2400 apparatus with nitrogen at 77 K. Assuming that the surface area of the silica flakes (ca. 3 $m^2\,g^{-1}$) is negligible and that the particles attached to them (the grains) are spherical, the particle size of dried and calcined films was evaluated, taking into account the weight percentage of oxides in the pigment samples, according to the following equation:

$$D\,(\mathrm{nm}) = \frac{6000\,f}{S_{\mathrm{BET}}\rho}$$

where f is the weight oxide fraction, S_{BET} is the BET surface area ($m^2\,g^{-1}$) and ρ is the bulk oxide density ($g\,cm^{-3}$). The values of the theoretical densities of the oxides that were used for the calculation were $d(Ta_2O_5)_{\beta\text{-Phase}} = 8.20\ g\,cm^{-3}$, $d(ZrO_2)_{\mathrm{tetragonal}} = 6.1\ g\,cm^{-3}$ and $d(TiO_2)_{\mathrm{anatase}} = 3.85\ g\,cm^{-3}$.

In fact, three types of grain size were deduced from these measurements. Crystallite size, grain size from SEM and grain size from BET. One should remind that the meaning and the associated precision differ from one to the other: G_{BET} and G_{crystal} are more precise at low temperature when particles are small and interparticle sintering can be neglected while G_{SEM} is more reliable at higher temperature. In all cases, the best accuracy that can be obtained from these methods is estimated to be 10 nm.[41]

3. Results

Cross sections of dried films (Ta140 and Zr140) are presented in Fig. 1. As it can be seen on these SEM micrographs, the powder layer is precipitated homogeneously and regularly onto the SiO_2 substrate. This was the case for all films investigated. The film thickness remains constant, with a precision of ±10 nm. The dried films were also investigated using light microscopy under transmission and reflection conditions. As an example, Ta60 pigments are shown in Fig. 2. In all cases, pigments appeared transparent, which denote their ability to scatter light as little as possible. It shows, macroscopically, the good quality of these pigments and the homogeneity of the layers. The films consist of oxide particles, which are called grains throughout this publication to make a clear distinction from the whole

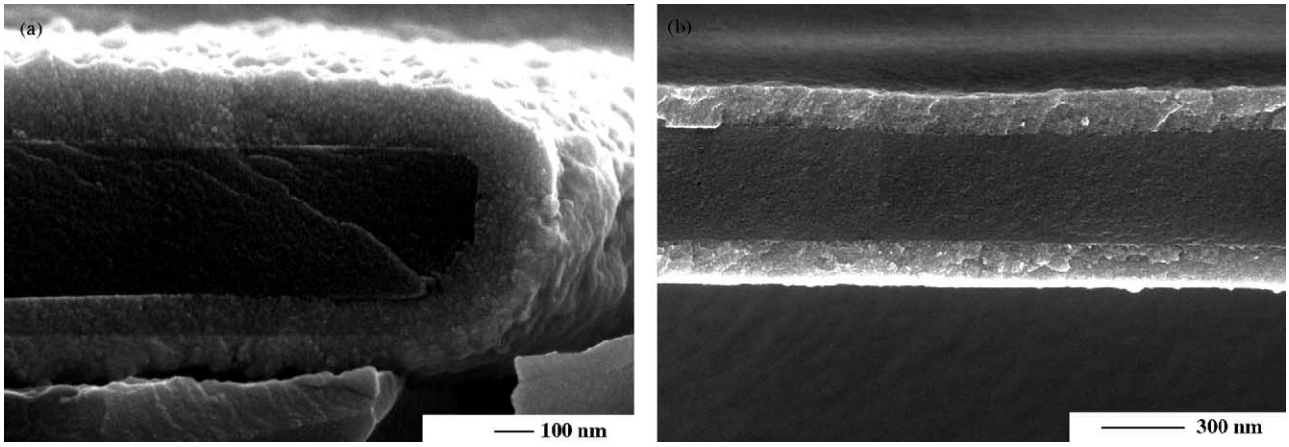

Fig. 1. SEM micrograph of cross sections of (a) Ta140 film and (b) Zr140 film.

particles themselves that consist of these films attached to substrates.

The dried samples were analyzed by TGA. A weight lost of 5% for Ta_2O_5 films (at 700 °C) and of 2% for ZrO_2 films (at 600 °C) was observed which was attributed to water departure. This experimental weight loss was significantly lower than that corresponding to the decomposition of hydroxides. It indicates that the precipitates were, in both cases, mainly oxides containing surface OH groups.

Figs. 3 and 4 present the evolution of X-ray diffractograms, respectively, of Ta140 film and the Zr140 film as a function of the calcination temperature.

The dried tantalum oxide film is actually X-ray amorphous and crystallization is noticeable only above 700–750 °C. Up to 1100 °C, the main phase is the orthorhombic tantalum oxide (β-Ta_2O_5, JCPDS file no. 25–922). A very similar crystallization process is obtained for Ta_2O_5 powder.

The dried zirconia film is also amorphous and crystallization takes place from 400 to 450 °C. At 950 °C, the main phase is tetragonal zirconium dioxide (*t*-ZrO_2, JCPDS file no. 50–1089) while a small amount of monoclinic phase is observed. The tetragonal phase represents about 90% of the volume of the layer as estimated from the surface area ratio of the $(\bar{1}11)_m$ and $(011)_t$ peaks. In the same manner, XRD analyses, performed on ZrO_2 precipitated powder, show that the dried powder is amorphous. Crystallization also occurs around 450 °C to give the tetragonal metastable phase but conversely to ZrO_2 films, the powder transforms into the monoclinic phase from 700 °C.

In the case of titania films deposited on mica, alumina or SiO_2 flakes, the layers are already crystallised after drying and present the anatase structure. This phase remains stable up to 1150 °C.[33] The dried titania powder, precipitated in the same conditions, is also obtained with the anatase structure but a phase transition from anatase to rutile is observed around 700 °C.

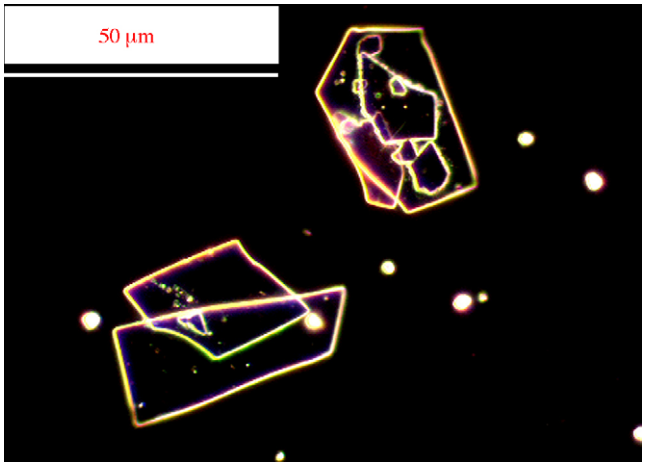

Fig. 2. Light microscopy images of Ta60 flakes (reflection stage—dark field).

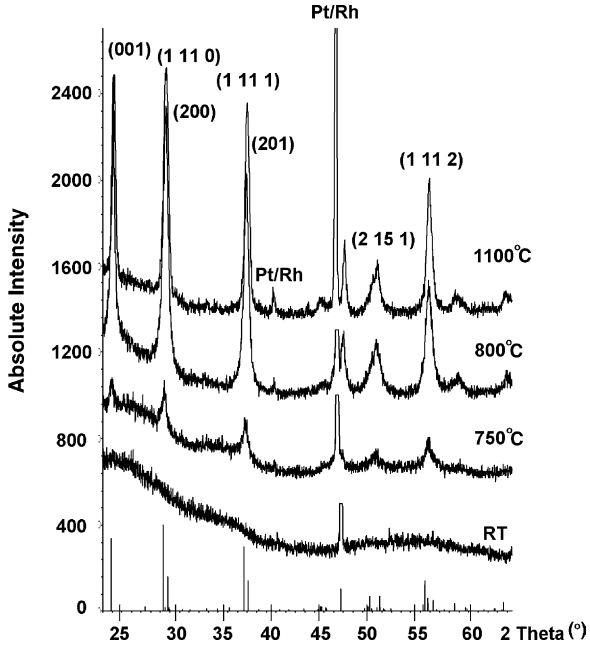

Fig. 3. Ta140 film crystallization process: in situ XRD patterns, performed under air, at room temperature (RT), 750, 800 and 1100 °C.

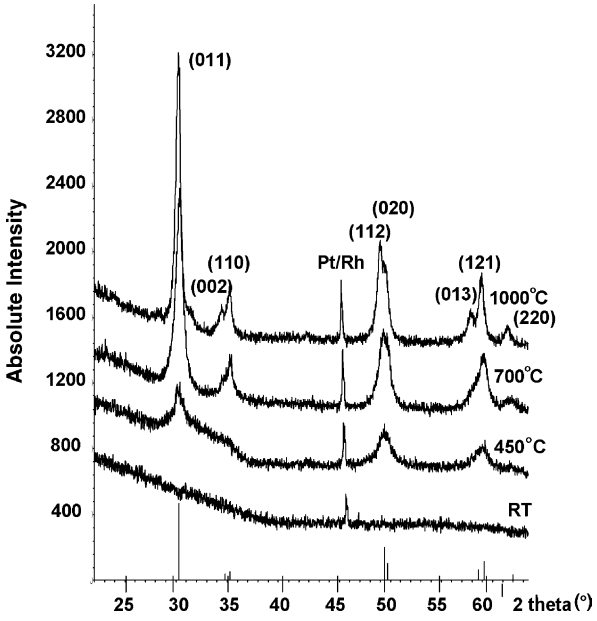

Fig. 4. Zr140 film crystallization process: in situ XRD patterns, performed under air, at room temperature (RT), 450, 700 and 1000 °C.

When the films are crystallised, crystallite size has been calculated from X-ray analyses and their evolution within the oxide films has been determined as a function of the calcination temperature (Figs. 5 and 6). Crystallite size within Ta_2O_5 films remains in the nanometric range and stays almost constant (∼25 nm) between 800 and 1200 °C. Crystallite size within ZrO_2 films is also clearly nanometric (∼10 nm at 500 °C) but a slight increase towards 20 nm is observed above 800 °C. Crystallite growth seems to be a little more pronounced for the thicker film.

BET isotherms of the films (dried at 110 °C or calcined at 600 and 900 °C) exhibited a type IV isotherm, according to the IUPAC classification.[42] The characteristic feature of this type is the hysteresis loop, which is associated to capillary condensation taking place in mesopores ($2 < d_p < 50$ nm). The expected saturation plateau at high pressure (H1 or H2 subtype hysteresis) is not observed which is attributed to the space present between single flakes, which behave like large slit-shaped pores. The pore volume has been then calculated from BET isotherms. As a matter of fact, pore volumes decrease as the calcination temperatures increase. A more precise analysis shows that micropores and mesopores are present in the dried films and that their relative proportion changes as the temperature increases. For all films, only mesopores remain present at 900 °C (Ta60 film = 0.039 $cm^3\,g^{-1}$, Ta140 film = 0.048 $cm^3\,g^{-1}$, Zr60 film = 0.020 $cm^3\,g^{-1}$, Zr140 film = 0.042 $cm^3\,g^{-1}$, Ti60 film = 0.012 $cm^3\,g^{-1}$, Ti140 film = 0.012 $cm^3\,g^{-1}$). Fig. 7 gives BET surface area of films and powders as a function of calcination temperature. As expected, surface area decrease as the calcination temperatures increase. However, the decrease of Ta_2O_5 film surface area arises at higher temperature than that of ZrO_2 films, indicating that sintering of these layers is retarded compared to zirconia films. Moreover, one should note that values of surface area of films remain significant at 900 °C and higher than powder's ones.

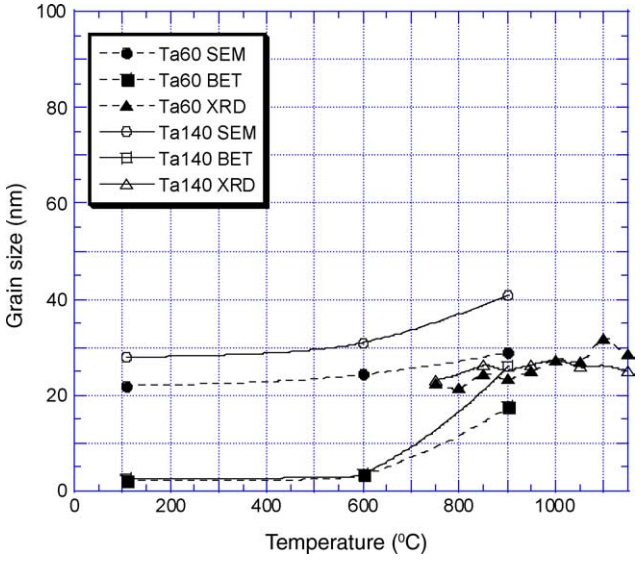

Fig. 5. Grain size within tantalum oxide films as a function of the measurement method and the calcination temperature.

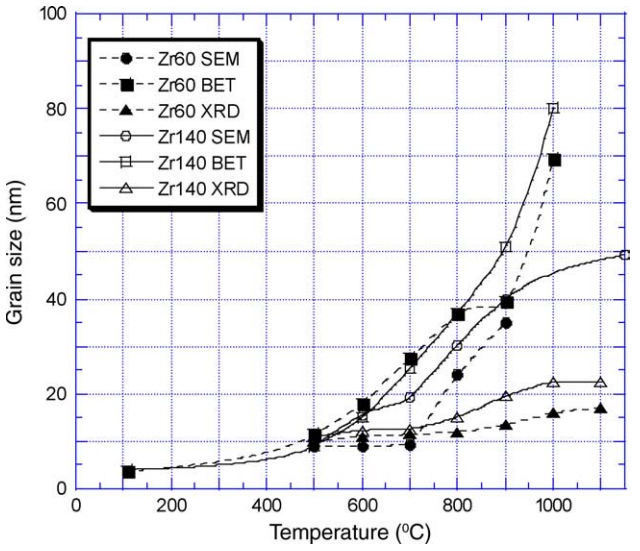

Fig. 6. Grain size within zirconia films as a function of the measurement method and the calcination temperature.

As explained in the experimental part, grain size has been calculated from BET measurements. These values are reported in Table 1 (and also in Figs. 5 and 6). Grain growth is observed for all types of sample. However, the tantalum and zirconium oxide films show a limited grain growth since final grain sizes (at 900 °C) remain less than 30 and 80 nm respectively. Ti140 sample presents a larger growth: at 700 °C, calculated grain size is higher than 200 nm; but initial grain size within the dried film was also an order of magnitude higher than in the other oxide films.[33]

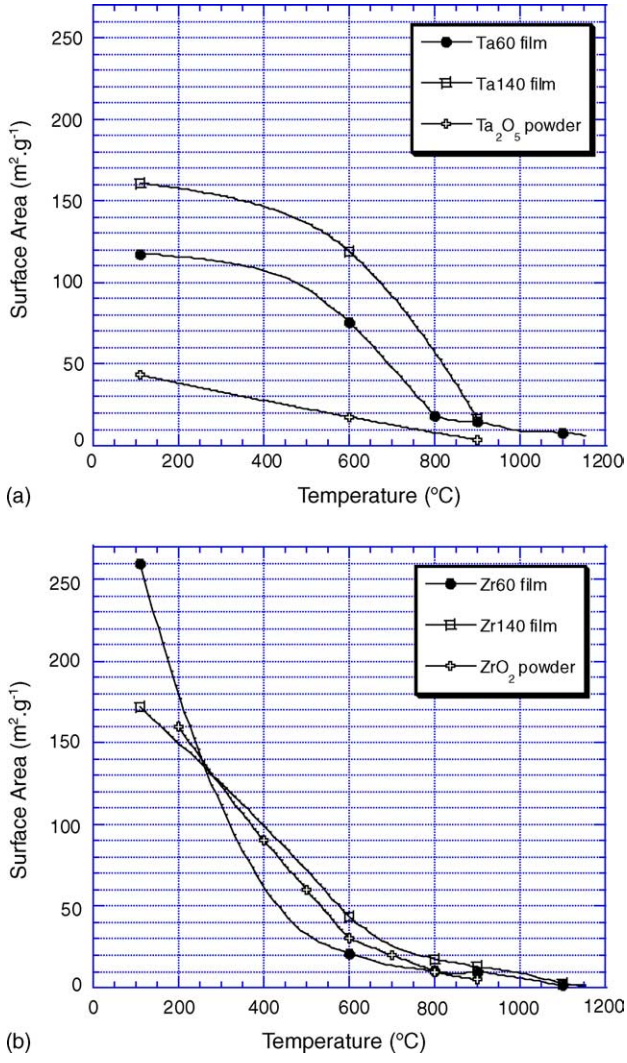

Fig. 7. BET surface area vs. calcination temperature for (a) Ta60, Ta140 films and Ta_2O_5 powder and (b) Zr60, Zr140 films and ZrO_2 powder.

Fig. 8 presents SEM images of the top surface of Ta60, Ta140 films and Ta_2O_5 powder after drying (110 °C) or calcination at 900 °C. Fig. 9 shows SEM top surface of Zr60 and Zr140 for the same conditions. Fig. 10 corresponds to Ti140 films. The surface of all specimens appears homogeneous excepted for the powder. For the samples dried at 110 °C (Figs. 8(a and c) and Fig. 9(a and c)) grain size of the dried pigments are clearly in the nanometric range in agreement with BET measurements. As the calcination temperature increases, grain size and pore size increases without any crack development. Comparing Fig. 8(a and c) and (b and d), one can also note that grain size looks larger within the thicker tantalum oxide layer. Such an observation seems to be in agreement with BET grain size calculations presented above (Table 1, Fig. 5) that indicated a difference of grain growth behavior between Ta60 and Ta140 from 800 °C. SEM micrographs of the reference Ti140 film, either dried or calcined at 900 °C for 30 min (Fig. 10) show that the grain growth process is even more marked than for tantalum oxide and zirconia films and no more porosity seems remaining in the layer.

4. Discussion

4.1. Structural evolutions

Crystallisation process appears to be different in the three studied systems. First, tantalum and zirconium oxide films are precipitated as amorphous products, while the reference titania films are already crystalline after drying at 110 °C. Second, the subsequent evolution for Ta_2O_5 films and ZrO_2 films differ. According to X-ray diffraction (Fig. 3), tantalum oxide films crystallized in the stable β phase at about 700 °C and show no other phase transformation in the investigated temperature range (<1100 °C). On the other hand, crystallization of zirconia films is noticeable from 400 to 450 °C and the metastable tetragonal phase is maintained up to 1000 °C (Fig. 4).

These differences are obviously related to the nature of the precipitated phases. But, the effect of the substrate on the thermal evolution of the film can already be mentioned. When tantalum oxide was precipitated without a substrate but using the same conditions as for the films, the same crystallographic behaviour was observed. On the other side, in zirconia and titania samples, crystalline evolution versus temperature is not the same for powders and films. For ZrO_2 powders, the tetragonal to monoclinic transformation takes place between 700 and 900 °C which is not observed for the films. For TiO_2, anatase precipitated titania powder shows a phase transition

Table 1
Calculated BET grain size as a function of the calcination temperature and green relative densities of films and bulk powders

Sample	G_{BET} (nm)			Relative density of the dried film (%)
	Dried	600 °C	900 °C	
Ta60 film	2.2	3.4	17.6	25
Ta140 film	2.7	3.6	26	29.6
Ta_2O_5 powder	16.9	41.5	208	70
Zr60 film	3.8	18	39.5	27.5
Zr140 film	5	15.1	50.8	39
ZrO_2 powder	5	11	50	53
Ti140 film	15	42	250[a]	68
TiO_2 powder	19.3	52.7	237	66

[a] This value means that the size of the grains have reached the thickness of the layer. It corresponds to an extension of the grains in the plane of the substrate.

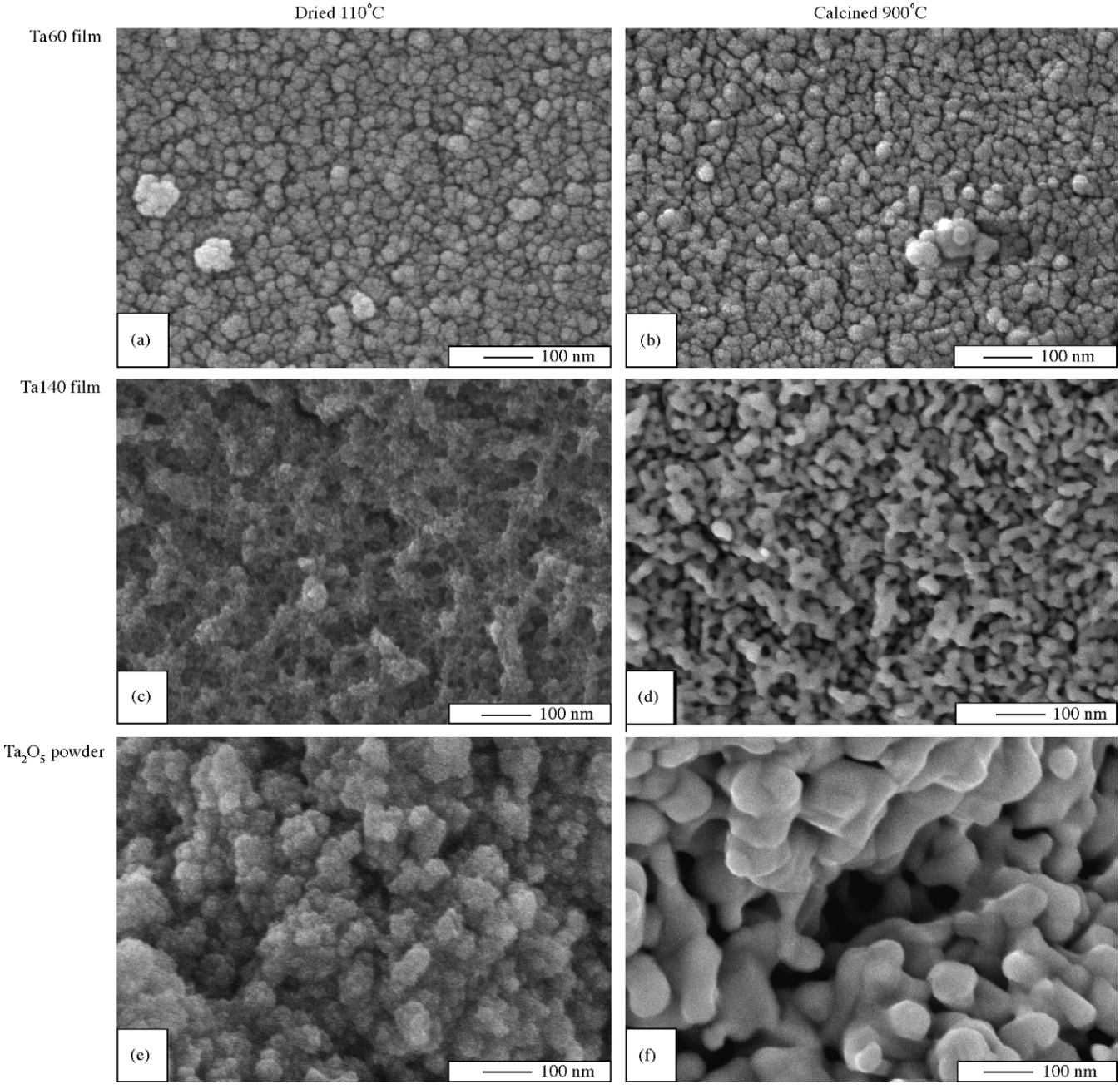

Fig. 8. SEM micrographs of Ta60, Ta140 films and of Ta_2O_5 powder, either in their dried state (a, c and e), or calcined at 900 °C (b, d and f).

from anatase to rutile at about 700 °C, while the anatase phase remains stable up to 1150 °C in the case of titania films deposited on mica, alumina or SiO_2 flakes.[33,43] In both cases, zirconia or titania, interactions between the powder layer and the stiff substrate limit the strong lattice contraction which retards the crystallographic transformation.

4.2. Microstructural evolution of tantalum and zirconium oxide films

Microstructural evolution of Ta_2O_5 and ZrO_2 films has been examined during calcination on the basis of three different techniques: nitrogen adsorption, XRD and SEM measurements. All the calculated grain sizes are reported respectively in Figs. 5 and 6.

Fig. 5 shows that, according to the BET measurements, Ta60 and Ta140 films behave in a similar manner below the crystallization of the tantalum oxide at 700 °C. For this low temperature range, SEM measurements give larger size which reveal agglomeration of the amorphous nanoparticles. At about 700 °C, crystallization occurs and grain growth takes place according to BET and SEM measurement methods. The fact that sizes obtained by BET and XRD measurements come close suggests that grains are monocrystalline without

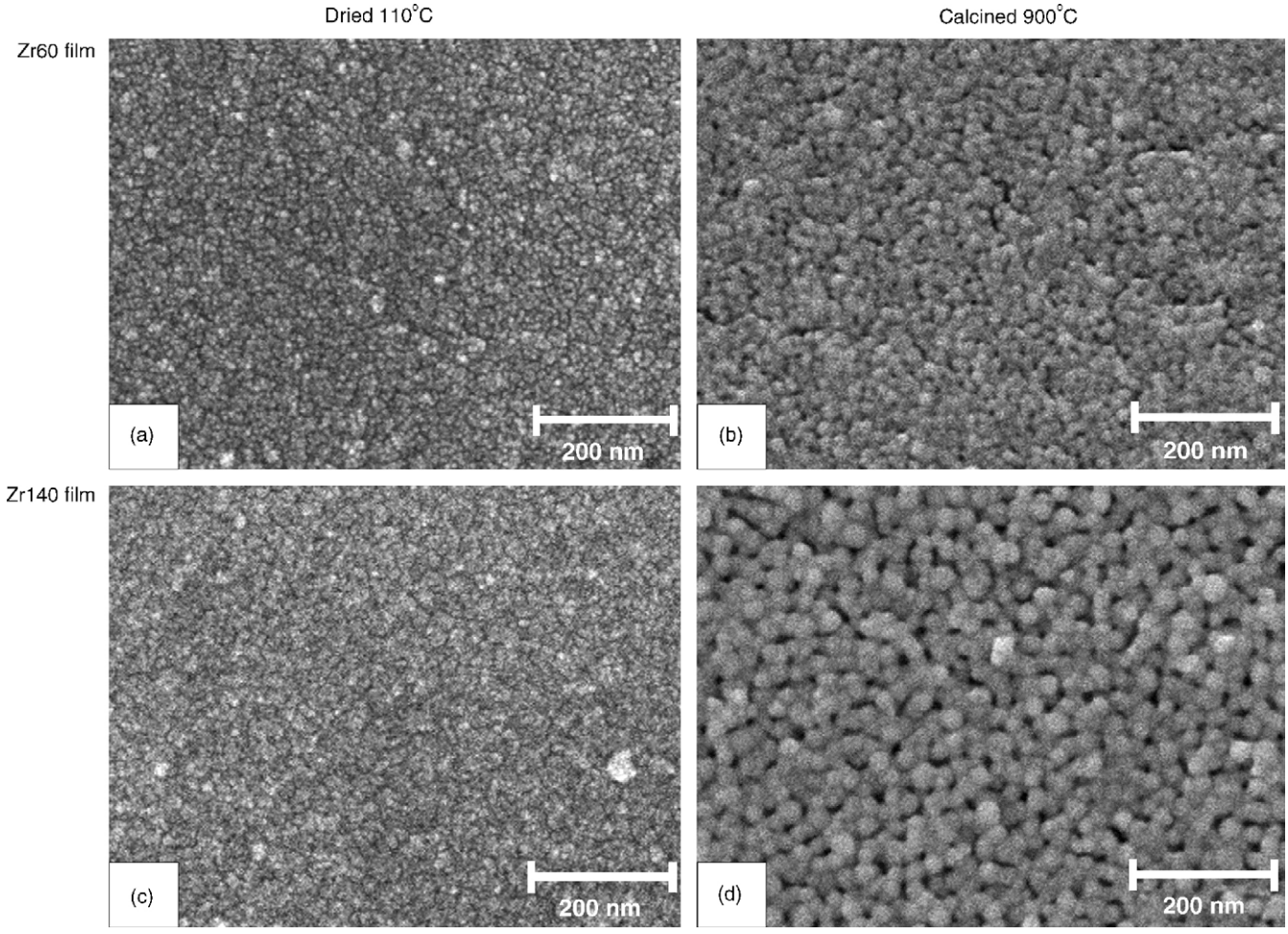

Fig. 9. SEM micrographs of Zr60 and Zr140 films either in their dried state (a and c), or calcined at 900 °C (b and d).

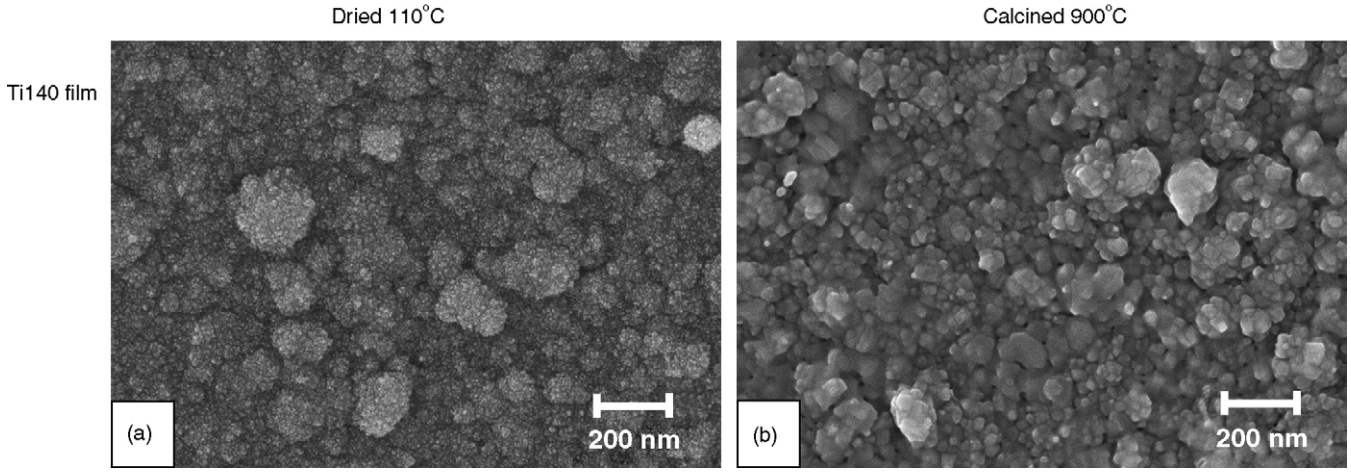

Fig. 10. SEM micrographs of Ti140 film: (a) dried at 110 °C and (b) calcined at 900 °C.

any internal pores; this is confirmed by BET isotherms that shows that there is no more micropore volume at 900 °C (only mesopores remain in the film at that temperature). So tantalum oxide films can be considered as made of agglomerates of initially amorphous particles and then monocrystalline grains whose sizes remain lower than 40 nm up to 1200 °C.

Fig. 6 presents grain growth behavior of zirconia films. Considering the typical errors mentioned in the experimental part, grain size evolution obtained from SEM and BET methods can be considered as practically identical up to ∼900 °C. Such correlation shows that the grains, observed on the SEM micrographs, do not contain a significant amount of internal pores (micropores with $d < 2$ nm). This is also seen directly from the low-temperature adsorption data. Then, XRD measurements shows that the size of the crystalline domains is always significantly smaller than the grain size calculated from nitrogen adsorption or shown on the SEM images. This difference proves that grains consist, all along the thermal treatment, of agglomerated crystallites which are not separated by pores. Preliminary TEM investigations performed on these samples lead to the same conclusions.[44] It means that zirconia films, when crystallized, are made of polycrystalline nanometric grains that grows up to 50–60 nm at 1200 °C.

Another point of interest deals with the influence of the film thickness on grain growth behavior. For Ta_2O_5 films, a slight difference of grain size is observed between the two films when SEM measurements were considered (Fig. 5). It could enter in the error bar (5–10 nm). For BET grain size, only the heat treatment at 900 °C leads to the same low difference between the two films. A way to characterize grain growth behavior as a function of temperature is to consider the grain growth factor (GGF) which is the ratio of the BET grains size at 900 °C to the initial BET grain size. In fact, the two values for Ta60 film and Ta140 film are very close: $GGF_{Ta60} = 8$ and $GGF_{Ta140} = 9.6$. So, we can consider that the grain growth process is about the same. Therefore, the slight difference in 900 °C grains size if it exists, could be attributed to small differences in the initial grain sizes. In the same manner, grains of Zr140 film heat treated at 900 °C look larger on SEM pictures (Fig. 9(d)) than Zr60 film grains (Fig. 9(b)). One can also note that according to XRD measurements (Fig. 6), crystallite size is always slightly larger for the thicker zirconia film. Since zirconia grains are polycrystalline, larger crystallite growth would result in a larger grain growth. But, calculation of GGF gives $GGF_{Zr60} = 8$ and $GGF_{Zr140} = 10.1$. These values are also quite close (considering the uncertainty of the measurements) which means that grain growth within these films can be considered as identical, like in the case of tantalum oxide films. Such a behavior is in agreement with other work related to grain growth within powder films.[45] When the size of grains within a powder film remains significantly lower than the film thickness, a normal 3D grain growth is expected. As a conclusion, grain growth within Ta_2O_5 and ZrO_2 films does not depend on the thickness of the films, since the size of grains remains lower than the film thickness. If some larger grain size are observed in the thicker films, it could be attributed to larger precipitated grains.

4.3. Influence of the substrate

As a first point, the densities of the dried tantalum and zirconium oxide films have been estimated from the pore volume taking into account microporosity and mesoporosity values deduced from adsorption measurements. These values are reported in Table 1. It appears that film densities are lower than the corresponding bulk powders. These low densities cannot be attributed to their amorphous state since the bulk powders are also amorphous but much denser. This difference can be related to the presence of the substrates during precipitation. For the two powder films, attachment of the initial nucleus to the substrate restrains the packing of grains. This effect is quite important due to the fact that the growth step, related to these syntheses, is weak as it is shown by the crystallite size of the dried products. Therefore, a porous layer is obtained and rearrangement or agglomeration is unlikely during drying, which can be obtained for the bulk powders.

In the case of titania, films and powders do not show that difference in green density. In fact, these samples are already crystalline at 110 °C and the grain size is also larger. The precipitation process is different and the growth step is favored compared to the previous case and the packing of the powder on the substrate is already good.

As a second point, grain growth evolution within Ta_2O_5 and ZrO_2 films has been compared to that of unsupported oxide powders. Grain sizes have been calculated from BET measurements and results for selected temperatures are presented in Table 1. Concerning Ta_2O_5 samples, grain size within bulk powders is always larger than that of films, all along the sintering process. The SEM micrographs presented on Fig. 10(f) confirms that, after heat treatment (900 °C), powder grains are larger than film grains. Now, grain growth is almost the same for the two types of samples. The value of the GGF of Ta_2O_5 powder, $GGF_{Ta_2O_5\ powder} = 12$, is only a little higher than the film values (8 and 9.6). It expresses that grain growth law is about the same; only the starting point is different. Concerning zirconia, the different samples present almost the same grain sizes as a function of temperature. The same grain growth is observed for the bulk powder and the films. The GGF value obtained for the bulk powder is $GGF_{ZrO_2\ powder} = 12$. This value is similar to Zr140 one. In fact, grain growth of Zr140 film and zirconia powders are also close to what was observed by Srdic for nanometric zirconia powders.[46] It confirms that grain growth within the films can be considered as normal grain growth. Therefore, in both cases, the influence of the substrate on grain growth appears limited. This has also been observed for alumina membranes sintered with and without a substrate.[47]

This is correlated with grain growth behavior of titania films and powders. In that case, the films are less porous and the same increase in grain size is observed when these sizes remain lower than the film thickness (at 600 °C for example).

When no thickness effect is present, normal grain growth are observed in these nanometric film samples.

Although synthesis conditions for these three types of oxides were quite similar, the size of the precipitated grains and the way they were packed onto the substrates were different enough to induce at higher temperatures the observed differences in grain size. For example, initial grain size is smaller within Ta_2O_5 films (Fig. 8) and ZrO_2 films (Fig. 9) compared to titania films (Fig. 10) and it remains larger during sintering. The grain growth behavior appears to be almost independent on the substrate. If the grain size remains lower than the thickness of the film, normal grain growth is observed.

5. Conclusions

The synthesis of thin tantalum and zirconium oxide layers deposited on amorphous silica substrates has been presented. Their sintering behaviour has been studied and compared to titania layers obtained from a similar synthesis method.

The control of experimental parameters allows the thickness of the well-defined inorganic layers to be adjusted between 50 and 150 nm. For tantalum oxide and zirconium oxide films, the precipitated grains are amorphous and their sizes range from 2 to 5 nm. After sintering, grain sizes remain in the nanometric range and are lower than the film thickness (from 30 to 40 nm). It was not the case for the reference titania layers where grain size reaches the film thickness. The amorphicity of tantalum oxide and zirconia retards grain growth up to the beginning of crystallization, while the crystallinity of precipitated titania grains favors their grain growth within the films.

Morphological evolution of the films during sintering depends on the nature of the oxide. The tantalum oxide films are constituted of agglomerates of initially amorphous grains that first crystallize to monocrystalline grains and then grow. The zirconia layer are made of polycrystalline grains and their growth corresponds to the growth of the elementary crystallites. Now, grain growth within these films, whatever their chemical nature, is not influenced by the film thickness.

The presence of the substrate does not affect the crystalline state of the precipitated nanometric particles. However, the substrate retards the phase transformation for the zirconia films as it has been previously observed for titania films. Concerning the effect of the substrate on sintering, it has a clear role on the packing of elementary particles during precipitation. This role is particularly strong for Ta_2O_5 films. Tantalum oxide and zirconia films are less dense than their powder counterpart. Grain growth within films is not affected by the presence of the substrate but the final sizes depend on the size of the initial precipitated grains. Titania deposition conditions gives dried layers constituted of larger grains that are better packed than equivalent Ta_2O_5 and ZrO_2 films. Then, grain size and density within tantalum and zirconium oxide layers are always lower than within titania layers.

Acknowledgements

The authors would like to thank Thierry Denaës, for the preparation and the optimization of the precipitation of Ta_2O_5 onto SiO_2 flakes. Dr. Martin Ermrich is gratefully acknowledged for the in situ XRD under air of the tantalum oxide samples (XRD Laboratory, Reinheim/Odw, Germany).

References

1. Kimura, H., Mizuki, J., Kamiyama, S. and Suzuki, H., Extended X-ray absorption fine structure analysis of the difference in local structure of tantalum oxide capacitor films produced by various annealing methods. *Appl. Phys. Lett.*, 1995, **66**, 2209–2211.
2. Yang, H., Tanoue, F., Hibino, S., Sakakibara, S., Yokoi, K. and Hotta, T., SrS: Ce thin films on different insulating underlayers. *Jpn. J. Appl. Phys.*, 1995, **34**, L757–L759.
3. Cevro, M. and Carter, G., Ion-beam and dual-ion-beam sputter deposition of tantalum oxide films. *Opt. Eng.*, 1995, **34**, 596–606.
4. Graham, D. W. and Stinton, D. P., Development of tantalum pentoxide coatings by chemical vapor deposition. *J. Am. Ceram. Soc.*, 1994, **77**, 2298–2304.
5. Harmsworth, P. D. and Stevens, R., Microstructure and zirconia-yttria plasma-sprayed thermal barrier coatings. *J. Mater. Res.*, 1992, **27**, 616–624.
6. Yunxia, C. and Weimin, L., Characterization and investigation of the tribological properties of sol–gel zirconia thin films. *J. Am. Ceram. Soc.*, 2002, **85**, 2367–2369.
7. Weimin, L., Yunxia, C., Chengfeng, Y. and Pingyu, Z., Preparation and characterization of doped sol–gel zirconia films. *Ceram. Int.*, 2002, **28**, 349–354.
8. Croset, M., Schnell, P., Valesco, G. J. and Sieja, J., Study of calcia-stabilized zirconia thin film sensors. *J. Vac. Sci. Technol.*, 1977, **14**, 777–781.
9. Sundeen, J. E. and Buchanan, R. C., Electrical properties of nickel-zirconia cermet films for temperature- and flow-sensor applications. *Sens. Actuators A Phys.*, 1997, **A63**, 33–40.
10. Peng, Z. and Liu, M., Preparation of dense platinum-yttria stabilized zirconia and yttria stabilized zirconia films on porous $La_{0.9}Sr_{0.1}MnO_3$ (LSM) substrates. *J. Am. Ceram. Soc.*, 2001, **84**, 283–288.
11. Ramanathan, S., McIntyre, P. C., Luning, J., Pianetta, P. and Muller, D. A., Structural studies of ultrathin zirconia dielectrics. *Philos. Mag. Lett.*, 2002, **82**, 519–528.
12. Maskalick, N. J. and Sun, C. C., Sintered zirconia electrolyte films in high-temperature fuel cells. *J. Electrochem. Soc.*, 1971, **118**, 1386–1391.
13. De Souza, S., Visco, S. J. and De Jonghe, L. C., Reduced-temperature solid oxide fuel cell based on YSZ thin-film electrolyte. *J. Electrochem. Soc.*, 1997, **144**, L35–L37.
14. Hobein, B., Tietz, F., Stover, D., Cekada, C. and Panjan, P., DC sputtering of yttria-stabilised zirconia films for solid oxide fuel cell applications. *J. Eur. Ceram. Soc.*, 2001, **21**, 1843–1846.
15. Basu, R. N., Randall, C. A. and Hayo, M. J., Fabrication of dense zirconia electrolyte films for tubular solid oxide fuel cells by electrophoretic deposition. *J. Am. Ceram. Soc.*, 2001, **84**, 33–40.
16. Pfaff, G. and Reynders, P., Angle-dependent optical effects deriving from submicron structures of films and pigments. *Chem. Rev.*, 1999, **99**, 1963–1981.
17. Greenstein, L. M., *Pigment Handbook, Vol. 1*, ed. P. E. Lewis. John Wiley & Sons, New York, 1988.
18. Franz, K. D., Emmert, R. and Nitta, K., Pearlescent pigments. *Kontakte (Darmstadt)*, 1992, **2**, 3–13.
19. Mollon, J. D., The origin of the concept of interference. *Philos. Trans. R. Soc. Lond.*, 2002, **A360**, 807–819.

20. Aoyama, T., Saida, S., Okayama, Y., Fujisaki, M., Imai, K. and Arikado, T., Leakage current mechanism of amorphous and polycrystalline Ta_2O_5 films grown chemical vapor deposition. *J. Electrochem. Soc.*, 1996, **143**, 977–983.
21. Koyama, H., Tanimoto, S., Kuroiwa, K. and Tarui, Y., Thermal properties of various Ta precursors used in chemical vapor deposition of tantalum pentoxide. *Jpn. J. Appl. Phys.*, 1994, **33**, 6291–6298.
22. Morstein, M., Pozsgai, I. and Spencer, N. D., Composition and microstructure of zirconia films obtained by MOCVD with a new, liquid, mixed acetylacetonato–alcoholato precursor. *Chem. Vap. Deposition*, 1999, **5**, 151–158.
23. Linton, H. R. (Du Pont), *Nacreous Pigment Compositions*. US Patent 3087828, 1963.
24. Linton, H. R. (Du Pont), *Micaceous Pigment Composition*. US Patent 3087829, 1963.
25. Quinn, C. A., Rieger, G. J. and Bolomey, R. A. (Mearl), *Method of Coating Surfaces with High Index Oxides*. US Patent 3437515, 1969.
26. Kohlschütter, H., Getrost, H., Reich, W., Rossler, H. and Horl, W. (Merck), *Process for Coating Titanium Dioxide on Solid Materials*. US Patent 3553001, 1971.
27. Osterried, K., Herbski, M. and Sage, I. (Merck), *Thermochromic Effect Pigment and Process for Producing the Same*. WO Patent 9312195, 1993.
28. Bauer, G., Osterried, K., Schmidt, C., Vogt, R., Kniess, H. B., Uhlig, M. *et al.*, *Coloured and Coated Platelike Pigments*. WO Patent 93/08237, 1991.
29. Scherrer, G. W. and Garino, T. J., Viscous sintering on a rigid substrate. *J. Am. Ceram. Soc.*, 1985, **68**, 216–220.
30. Garino, T. J. and Bowen, H. K., Kinetics of constrained-film sintering. *J. Am. Ceram. Soc.*, 1990, **73**, 251–257.
31. Lange, F. F. and Miller, K. T., The instability of polycrystalline thin films: experiment and theory. *J. Mater. Res.*, 1990, **5**, 151–160.
32. Hildenbrand, V. D., Doyle, S., Fuess, H., Pfaff, G. and Reynders, P., Crystallization of thin anatase coatings on muscovite. *Thin Solid Films*, 1997, **304**, 204–211.
33. Stech, M., Reynders, P. and Rödel, J., Constrained film sintering of nanocrystalline TiO_2. *J. Am. Ceram. Soc.*, 2000, **83**, 1889–1896.
34. Stech, M. and Reynders, P., Preparation and characterization of thin metal oxide layers used for producing angle-dependent optical effects. In *Emulsion, Foams and Thin Films*, ed. K. L. Mittal. Marcel Dekker Inc, Basel, 2000, pp. 447–461.
35. Dehn, J., Buschmann, V., Reynders, P. and Fuess, H., Orientation relationships of hematite layers on ceramic substrates. In *Proceeding of the 19th European Crystallographic Meeting, 207*, 2000.
36. Legallee, C. R. (Flex Products Inc), *Optically Variable Pigments and Foils with Enhanced Color Shifting Properties*. WO Patent 02/24818, 2000.
37. Kolodziej, R. and Simon, J. C. (LĭOréal), *Foundation Composition Containing Interference Pigments*. WO Patent 03/020225, 2001.
38. Speer, D., Zell, C., Wilfert, J. and Kiss, A. (Cerdec AG), *Violet Zircon Vanadium Pigments*. European Patent 0616974, 1994.
39. Nitta, K., Watanabe, T. and Suzuki, I. (Merck), *Water Resistant Nacreous Pigment and Process for Producing the Same*. US Patent 4828623, 1983.
40. Nitta, K. and Suzuki, I. (Merck), *Weather-resistant, Pearlescent Pigment and Process for Producing the Same in the Presence of Hypophosphite*. US Patent 5223034, 1988.
41. Bertaux, S., *Synthesis of Well Defined Inorganic Layers Using Fluidized Bed*. Ph.D. thesis, University Bordeaux 1, no. 2711, 2003.
42. Sing, K. S. W., Everett, D. H., Haul, R. A. W., Moscou, L., Pierotti, A., Rouquerol, J. *et al.*, Reporting physisorption data for gas/solid systems with special reference to the determination of surface area and porosity (Recommendations 1984). *Pure Appl. Chem.*, 1985, **57**, 603–619.
43. Stech, M., *Sintern von nanokristallinen Titandioxidfilmen mit geometrischen Einschränkungen*. Ph.D. thesis, Technical University of Darmstadt, Germany, 1999.
44. Knoth, M., Miehe, G. and Fuess, H. Adv. Eng. Mater., submitted for publication.
45. Thompson, C. V., Grain growth in thin films. *Annu. Rev. Mater. Sci.*, 1990, **20**, 245–268.
46. Srdic, V. V., Winterer, M. and Hahn, H., Sintering behavior of nanocrystalline zirconia prepared by chemical vapor synthesis. *J. Am. Ceram. Soc.*, 2000, **83**, 729–736.
47. Levänen, E. and Mäntyla, T., Effect of sintering temperature on functional properties of alumina membranes. *J. Eur. Ceram. Soc.*, 2002, **22**, 613–623.